Editors' Suggestion | Featured in Physics

Temporal Structures in Electron Spectra and Charge Sign Effects in Galactic Cosmic Rays

M. Aguilar,[29] L. Ali Cavasonza,[1] G. Ambrosi,[36] L. Arruda,[27] N. Attig,[24] C. Bagwell,[10] F. Barao,[27] L. Barrin,[15] A. Bartoloni,[40] S. Başeğmez-du Pree,[18,*] R. Battiston,[47,48] M. Behlmann,[10] N. Belyaev,[10] J. Berdugo,[29] B. Bertucci,[36,37] V. Bindi,[20] K. Bollweg,[21] J. Bolster,[10] B. Borgia,[40,41] M. J. Boschini,[31] M. Bourquin,[16] E. F. Bueno,[18] J. Burger,[10] W. J. Burger,[47] S. Burmeister,[25] X. D. Cai,[10] M. Capell,[10] J. Casaus,[29] G. Castellini,[14] F. Cervelli,[38] Y. H. Chang,[45] G. M. Chen,[6,7] G. R. Chen,[23] H. S. Chen,[6,7] Y. Chen,[16,23] L. Cheng,[23] H. Y. Chou,[45] S. Chouridou,[1] V. Choutko,[10] C. H. Chung,[1] C. Clark,[10,21] G. Coignet,[3] C. Consolandi,[20] A. Contin,[8,9] C. Corti,[20] Z. Cui,[22,23] K. Dadzie,[10] A. Dass,[47,48] C. Delgado,[29] S. Della Torre,[31] M. B. Demirköz,[2] L. Derome,[17] S. Di Falco,[38] V. Di Felice,[42] C. Díaz,[29] F. Dimiccoli,[47] P. von Doetinchem,[20] F. Dong,[34] F. Donnini,[36] M. Duranti,[36] A. Egorov,[10] A. Eline,[10] F. Faldi,[36,37] J. Feng,[10] E. Fiandrini,[36,37] P. Fisher,[10] V. Formato,[42] C. Freeman,[20] C. Gámez,[29] R. J. García-López,[26] C. Gargiulo,[15] H. Gast,[1] M. Gervasi,[31,32] F. Giovacchini,[29] D. M. Gómez-Coral,[20] J. Gong,[34] C. Goy,[3] V. Grabski,[30] D. Grandi,[31,32] M. Graziani,[36,37] A. N. Guracho,[40] S. Haino,[45] K. C. Han,[28] R. K. Hashmani,[2] Z. H. He,[19] B. Heber,[25] T. H. Hsieh,[10] J. Y. Hu,[6,7] M. Incagli,[38] W. Y. Jang,[13] Yi Jia,[10] H. Jinchi,[28] G. Karagöz,[2] B. Khiali,[42] G. N. Kim,[13] Th. Kirn,[1] O. Kounina,[10] A. Kounine,[10] V. Koutsenko,[10] D. Krasnopevtsev,[10] A. Kuhlman,[20] A. Kulemzin,[10] G. La Vacca,[31,32] E. Laudi,[15] G. Laurenti,[8] G. LaVecchia,[10] I. Lazzizzera,[47,48] H. T. Lee,[44] S. C. Lee,[45] H. L. Li,[23] J. Q. Li,[34] M. Li,[1] Q. Li,[34] Q. Y. Li,[23] S. Li,[1] S. L. Li,[6,7] J. H. Li,[22] Z. H. Li,[6,7] J. Liang,[22] M. J. Liang,[6,7] C. Light,[20] C. H. Lin,[45] T. Lippert,[24] J. H. Liu,[5] S. Q. Lu,[45] Y. S. Lu,[6] K. Luebelsmeyer,[1] J. Z. Luo,[34] Xi Luo,[23] F. Machate,[1] C. Mañá,[29] J. Marín,[29] J. Marquardt,[25] T. Martin,[10,21] G. Martínez,[29] N. Masi,[8] D. Maurin,[17] T. Medvedeva,[10] A. Menchaca-Rocha,[30] Q. Meng,[34] V. V. Mikhailov,[33] M. Molero,[26] P. Mott,[10,21] L. Mussolin,[36,37] J. Negrete,[20] N. Nikonov,[1] F. Nozzoli,[47] J. Ocampo-Peleteiro,[29] A. Oliva,[8] M. Orcinha,[27] M. Palermo,[20] F. Palmonari,[8,9] M. Paniccia,[16] A. Pashnin,[10] M. Pauluzzi,[36,37] S. Pensotti,[31,32] V. Plyaskin,[10] M. Pohl,[16] S. Poluianov,[35] X. Qin,[10] Z. Y. Qu,[23] L. Quadrani,[8,9] P. G. Rancoita,[31] D. Rapin,[16] A. Reina Conde,[8] E. Robyn,[16] S. Rosier-Lees,[3] A. Rozhkov,[10] D. Rozza,[31] R. Sagdeev,[11] S. Schael,[1] A. Schultz von Dratzig,[1] G. Schwering,[1] E. S. Seo,[12] B. S. Shan,[4] T. Siedenburg,[1] J. W. Song,[22] X. J. Song,[23] R. Sonnabend,[1] L. Strigari,[40,†] T. Su,[23] Q. Sun,[22] Z. T. Sun,[6,7] M. Tacconi,[31,32] X. W. Tang,[6] Z. C. Tang,[6] J. Tian,[42] Samuel C. C. Ting,[10,15] S. M. Ting,[10] N. Tomassetti,[36,37] J. Torsti,[49] T. Urban,[10,21] I. Usoskin,[35] V. Vagelli,[39,36] R. Vainio,[49] M. Valencia-Otero,[46] E. Valente,[40,41] E. Valtonen,[49] M. Vázquez Acosta,[26] M. Vecchi,[18] M. Velasco,[29] J. P. Vialle,[3] C. X. Wang,[22] L. Wang,[5] L. Q. Wang,[22] N. H. Wang,[22] Q. L. Wang,[5] S. Wang,[20] X. Wang,[10] Yu Wang,[22] Z. M. Wang,[23] J. Wei,[16,23] Z. L. Weng,[10] H. Wu,[34] R. Q. Xiong,[34] W. Xu,[22,23] Q. Yan,[10] Y. Yang,[43] I. I. Yashin,[33] A. Yelland,[10] H. Yi,[34] Y. M. Yu,[10] Z. Q. Yu,[6] M. Zannoni,[31,32] C. Zhang,[6] F. Zhang,[6] F. Z. Zhang,[6,7] J. H. Zhang,[34] Z. Zhang,[10] F. Zhao,[6,7] C. Zheng,[23] Z. M. Zheng,[4] H. L. Zhuang,[6] V. Zhukov,[1] A. Zichichi,[8,9] and P. Zuccon[47,48]

(AMS Collaboration)

[1]*I. Physics Institute and JARA-FAME, RWTH Aachen University, 52056 Aachen, Germany*
[2]*Department of Physics, Middle East Technical University (METU), 06800 Ankara, Turkey*
[3]*Université Grenoble Alpes, Université Savoie Mont Blanc, CNRS, LAPP-IN2P3, 74000 Annecy, France*
[4]*Beihang University (BUAA), Beijing 100191, China*
[5]*Institute of Electrical Engineering (IEE), Chinese Academy of Sciences, Beijing 100190, China*
[6]*Institute of High Energy Physics (IHEP), Chinese Academy of Sciences, Beijing 100049, China*
[7]*University of Chinese Academy of Sciences (UCAS), Beijing 100049, China*
[8]*INFN Sezione di Bologna, 40126 Bologna, Italy*
[9]*Università di Bologna, 40126 Bologna, Italy*
[10]*Massachusetts Institute of Technology (MIT), Cambridge, Massachusetts 02139, USA*
[11]*East–West Center for Space Science, University of Maryland, College Park, Maryland 20742, USA*
[12]*IPST, University of Maryland, College Park, Maryland 20742, USA*
[13]*CHEP, Kyungpook National University, 41566 Daegu, Korea*
[14]*CNR–IROE, 50125 Firenze, Italy*
[15]*European Organization for Nuclear Research (CERN), 1211 Geneva 23, Switzerland*
[16]*DPNC, Université de Genève, 1211 Genève 4, Switzerland*
[17]*Université Grenoble Alpes, CNRS, Grenoble INP, LPSC-IN2P3, 38000 Grenoble, France*

[18]Kapteyn Astronomical Institute, University of Groningen, P.O. Box 800, 9700 AV Groningen, Netherlands
[19]Sun Yat–Sen University (SYSU), Guangzhou, 510275, China
[20]Physics and Astronomy Department, University of Hawaii, Honolulu, Hawaii 96822, USA
[21]National Aeronautics and Space Administration Johnson Space Center (JSC), Houston, Texas 77058, USA
[22]Shandong University (SDU), Jinan, Shandong 250100, China
[23]Shandong Institute of Advanced Technology (SDIAT), Jinan, Shandong 250100, China
[24]Jülich Supercomputing Centre and JARA-FAME, Research Centre Jülich, 52425 Jülich, Germany
[25]Institut für Experimentelle und Angewandte Physik, Christian-Alberts-Universität zu Kiel, 24118 Kiel, Germany
[26]Instituto de Astrofísica de Canarias (IAC), 38205 La Laguna, Tenerife, Spain and Departamento de Astrofísica, Universidad de La Laguna, 38206 La Laguna, Tenerife, Spain
[27]Laboratório de Instrumentação e Física Experimental de Partículas (LIP), 1649-003 Lisboa, Portugal
[28]National Chung–Shan Institute of Science and Technology (NCSIST), Longtan, Tao Yuan 32546, Taiwan
[29]Centro de Investigaciones Energéticas, Medioambientales y Tecnológicas (CIEMAT), 28040 Madrid, Spain
[30]Instituto de Física, Universidad Nacional Autónoma de México (UNAM), Ciudad de México, 01000 Mexico
[31]INFN Sezione di Milano–Bicocca, 20126 Milano, Italy
[32]Università di Milano–Bicocca, 20126 Milano, Italy
[33]NRNU MEPhI (Moscow Engineering Physics Institute), Moscow, 115409 Russia
[34]Southeast University (SEU), Nanjing 210096, China
[35]Sodankylä Geophysical Observatory and Space Physics and Astronomy Research Unit, University of Oulu, 90014 Oulu, Finland
[36]INFN Sezione di Perugia, 06100 Perugia, Italy
[37]Università di Perugia, 06100 Perugia, Italy
[38]INFN Sezione di Pisa, 56100 Pisa, Italy
[39]Agenzia Spaziale Italiana (ASI), 00133 Roma, Italy
[40]INFN Sezione di Roma 1, 00185 Roma, Italy
[41]Università di Roma La Sapienza, 00185 Roma, Italy
[42]INFN Sezione di Roma Tor Vergata, 00133 Roma, Italy
[43]National Cheng Kung University, Tainan 70101, Taiwan
[44]Academia Sinica Grid Center (ASGC), Nankang, Taipei 11529, Taiwan
[45]Institute of Physics, Academia Sinica, Nankang, Taipei 11529, Taiwan
[46]Physics Department and Center for High Energy and High Field Physics, National Central University (NCU), Tao Yuan 32054, Taiwan
[47]INFN TIFPA, 38123 Trento, Italy
[48]Università di Trento, 38123 Trento, Italy
[49]Space Research Laboratory, Department of Physics and Astronomy, University of Turku, 20014 Turku, Finland

(Received 22 September 2022; revised 21 November 2022; accepted 9 February 2023; published 17 April 2023)

We present the precision measurements of 11 years of daily cosmic electron fluxes in the rigidity interval from 1.00 to 41.9 GV based on 2.0×10^8 electrons collected with the Alpha Magnetic Spectrometer (AMS) aboard the International Space Station. The electron fluxes exhibit variations on multiple timescales. Recurrent electron flux variations with periods of 27 days, 13.5 days, and 9 days are observed. We find that the electron fluxes show distinctly different time variations from the proton fluxes. Remarkably, a hysteresis between the electron flux and the proton flux is observed with a significance of greater than 6σ at rigidities below 8.5 GV. Furthermore, significant structures in the electron-proton hysteresis are observed corresponding to sharp structures in both fluxes. This continuous daily electron data provide unique input to the understanding of the charge sign dependence of cosmic rays over an 11-year solar cycle.

DOI: 10.1103/PhysRevLett.130.161001

Introduction.—Cosmic rays are dominated by positively charged particles and nuclei: protons, helium, etc. Electrons are the most abundant negatively charged particles, but cosmic electrons are rare. The precision study of cosmic electrons requires a magnetic spectrometer in space to separate electrons from positrons and the overwhelming number of positively charged protons and nuclei.

Since installation on the International Space Station on May 20, 2011, AMS has continuously collected and analyzed electron events daily. Most of these events (around 99%) are in the low rigidity range below

41.9 GV. The high rigidity 1% of the spectrum up to 2 TeV provides unexpected results, which will be presented in a future publication.

The fluxes of charged cosmic rays outside the heliosphere are thought to be stable on the timescale of decades [1–4]. Time-dependent variations in the fluxes of galactic cosmic rays measured inside the heliosphere are only expected from the solar modulation [5]. Solar modulation involves convective, diffusive, particle drift, and adiabatic energy loss processes [6]. Only particle drift induces a dependence of solar modulation on the particle charge sign [7]. The systematic measurement of the electron flux and the proton flux offers a unique way to study charge-sign-dependent solar modulation effects.

Cosmic electrons are primary cosmic rays [8]. Their time structure is of particular importance as electrons have been widely used to search for new phenomena in primary cosmic rays, such as the existence of nearby pulsars [9], supernovae remnants [10], or dark matter annihilation [11,12]. Models describing these phenomena can only be compared to data when time-dependent effects in the heliosphere are well understood [13–16]. A comprehensive model of the time-dependent solar modulation will have far-reaching consequences for the understanding of the newly observed unexpected features in cosmic-ray fluxes, such as the complex energy dependence of the positron spectrum [17] and of the electron spectrum [18], as well as for other domains of astrophysics, such as the modeling of galactic cosmic-ray propagation [19], the estimate of the galactic cosmic-ray pressure, an important ingredient for models of galaxy formation [20], the interpretation of possible anisotropies in the cosmic-ray arrival directions at the Earth [21], and the understanding of cosmic-ray spectra outside the solar system [22].

Previous experiments measured the time variation of the combined (electron + positron) flux [23–26], the electron flux variation averaged over six- and three-month periods [27], or averaged over two days for a total of two months [28]. AMS has reported the time dependence of the electron fluxes and the positron fluxes per Bartels rotations (BR: 27 days) over six years [29]. In addition, AMS has observed short-term structures in the cosmic-ray proton flux [30] and helium flux [31].

In this Letter, we present the daily electron fluxes based on 2.0×10^8 events spanning 11 years over a rigidity range from 1.00 to 41.9 GV. These data cover the major portion of solar cycle 24, which includes the polarity reversal of the solar magnetic field in the year 2013 [32], and the beginning of solar cycle 25. Therefore, the charge-sign-dependent effects are studied at different solar conditions by comparing the daily electron and daily proton [30] fluxes measured simultaneously over an 11-year period. These data provide unique and accurate input to modeling of the transport processes of charged cosmic rays inside the heliosphere.

Detector.—The layout and description of the AMS detector are presented in Refs. [8,33] and shown in Fig. S1 of the Supplemental Material (SM) [34]. The key elements used in this measurement are the permanent magnet [35], the silicon tracker [36–38], the transition radiation detector (TRD) [39], the four planes of time-of-flight (TOF) scintillation counters [40], and the electromagnetic calorimeter (ECAL) [41]. Further information on the AMS layout, performance, trigger, and the Monte Carlo (MC) simulation [42,43] is detailed in the SM [34].

Event selection.—AMS has collected 1.9×10^{11} cosmic-ray events. In the rigidity range from 1.00 to 41.9 GV, we select electron samples using the combined information of the TRD, TOF, and inner tracker. The details of the event selection and backgrounds are contained in Refs. [17,18,44–46] and in the SM [34]. After selection, we obtained 2.0×10^8 electrons.

Data analysis.—The daily isotropic flux in the ith absolute rigidity bin $(R_i, R_i + \Delta R_i)$ and jth day is given by

$$\Phi_i^j = \frac{N_i^j}{A_i^j(1+\delta_i^j)\epsilon_i^j T_i^j \Delta R_i}, \tag{1}$$

where N_i^j is the number of events corrected for background and bin-to-bin migration; A_i^j is the effective acceptance calculated from the Monte Carlo simulation, including geometric acceptance, event selection efficiencies, and interactions of electrons in the AMS materials; δ_i^j is the small correction to the acceptance due to the difference in the event selection efficiencies between data and Monte Carlo simulation; ϵ_i^j is the trigger efficiency; and T_i^j is the daily collection time. See the SM [34], Figs. S2 and S3, for more details. In this Letter, the electron flux is measured in ten rigidity bins from 1.00 to 41.9 GV.

The background contribution from antiprotons and light mesons in the data sample is estimated using a template fit to the distribution of TRD estimator Λ_{TRD} [8]. The background contribution from charge confusion positrons is estimated to be negligible [8].

Bin-to-bin migration of events is corrected using the unfolding procedures described in Ref. [47].

The small corrections δ_i^j are estimated by comparing the efficiencies in data and Monte Carlo simulation of every selection cut using information from the detectors unrelated to that cut. The δ_i^j are found to have a small rigidity dependence: from −5% at 1 GV, decreasing to −2.4% at 10 GV, and becoming constant at −2.8% above 30 GV.

There are extensive studies of the systematic errors. These errors include the uncertainties in the templates definition, the trigger efficiency, the geomagnetic cutoff, the acceptance calculation, the rigidity resolution function, the unfolding, and the absolute rigidity scale.

The uncertainty associated with the Λ_{TRD} templates definition includes two parts: the event selection and the

statistical fluctuations [18]. These two errors are added in quadrature. The time-dependent systematic error due to the templates definition amounts to less than 0.5% of the flux below 41.9 GV.

The time-dependent systematic error on the electron fluxes associated with the trigger efficiency measurement is less than 1% over the entire rigidity range and for all days.

The geomagnetic cutoff is calculated as described in the SM [34], and the resulting systematic error on the fluxes is less than 2% at 1 GV and negligible (less than 0.4%) above 2 GV.

The correction δ_i^j is stable with time within its error, and the associated time-dependent systematic error on the fluxes is less than 1.5% over the entire rigidity range for all days.

The time-independent rigidity resolution function for electrons has a pronounced Gaussian core and non-Gaussian tails. The systematic error on the fluxes due to the rigidity resolution function is obtained by repeating the unfolding procedure while independently varying the width of the Gaussian core by 5% and the amplitude of the non-Gaussian tails by 10% [47]. The resulting systematic error on the fluxes is 2% at 1 GV and less than 1% above 2 GV.

The daily variation of the spectral shape leads to an additional uncertainty in the unfolding procedure. The resulting time-dependent systematic error is less than 1% at 1 GV and is negligible (less than 0.2%) above 5 GV for all days.

There are two contributions to the systematic uncertainty on the rigidity scale [47]. The first is due to residual tracker misalignment. This error is estimated by comparing the E/p ratio for electrons and positrons, where E is the energy measured with the electromagnetic calorimeter and p is the momentum measured with the tracker. It is found to be $1/30$ TV [48]. The error is negligible (less than 0.2%) below 41.9 GV. The second systematic error on the rigidity scale arises from the magnetic field map measurement and its temperature corrections. The total time-independent error on the fluxes due to uncertainty on the rigidity scale has been calculated to be less than 0.5% over the rigidity range below 41.9 GV.

The contributions to the systematic error from the trigger efficiency, the reconstruction efficiencies, and the unfolding are evaluated independently each day and are added in quadrature to derive a time-dependent systematic error, which is less than 2% at 1 GV and about 1% above 3 GV for all days.

The daily total systematic error is obtained by adding in quadrature the individual contributions of the time-independent systematic errors discussed above and the time-dependent systematic errors. At 1 GV, it is less than 3%, and above 3 GV, it is about 1.5% for all days.

Most importantly, several independent analyses were performed on the same data sample by different study groups. The results of those analyses are consistent with this Letter.

Results.—The daily electron fluxes (Φ_{e^-}) including statistical errors, time-dependent systematic errors, and total systematic errors are tabulated in Tables S1–S3300 of the SM [34,49] as functions of the rigidity at the top of the AMS detector. These daily data are in agreement with our earlier 27-day results [29] in the overlapping time period but with improved accuracy. The daily proton flux (Φ_p) data from May 2011 to November 2019 are taken from Ref. [30]. The new Φ_p data up to November 2021 will be published separately.

Figure 1 shows Φ_{e^-} and Φ_p for four rigidity bins from 1.00 to 11.0 GV; see also Fig. S6 of the SM [34] for Φ_{e^-} in circular format. In this and subsequent figures, the error bars on the fluxes are the quadratic sum of the statistical and time-dependent systematic errors. As seen, Φ_{e^-} exhibits both short-term variations on the scale of days to months and long-term variations on the scale of years, and the relative magnitude of these variations decreases with increasing rigidity. The time-dependent behavior of the Φ_{e^-} and Φ_p is distinctly different, and the differences decrease with increasing rigidity. From 2011 to 2014, Φ_{e^-} decreases faster with time than Φ_p. From 2015 to mid-2017, Φ_{e^-} increase more slowly than Φ_p below about 4 GV [Figs. 1(a) and 1(b)]. From mid-2020 to 2021, Φ_{e^-} decreases faster than Φ_p.

Short-term flux variations can be either recurrent or nonrecurrent. The nonrecurrent variations are mainly caused by transient disturbances in the interplanetary magnetic field [26,28,30,31,50,51]. The comparison of the nonrecurrent variation of daily Φ_{e^-} and Φ_p for three short time intervals is shown in Fig. S7 of the SM [34]. As seen, during lower solar activity (left and right columns of Fig. S7), a difference between the short-term evolution of electrons and protons is observed, while during the solar maximum (middle column of Fig. S7), the difference vanishes. For instance, in Figs. S7(b) and S7(j), the slope of the recovery after the dip is different between electrons and protons. These observations indicate a charge-sign dependence in nonrecurrent solar modulation.

Recurrent variations with a period of 27 days and its harmonics are related to solar rotation [52–60]. To study the recurrent variations in Φ_{e^-}, a wavelet time-frequency technique [61] was used to locate the time intervals where the periodic structures emerge. The details on the wavelet analysis are described in the SM [34]. All the power spectra in the subsequent figures are drawn with normalized power defined in the SM [34]. The Φ_{e^-} for four rigidity intervals from 1.00 to 11.0 GV in each year (2011–2021 defined in Table SA of the SM [34]), together with their time-averaged power spectra and 95% confidence levels, are shown in Figs. S8–S18 of the SM [34].

The peak values of the normalized power around 27 days, 13.5 days, and 9 days as a function of rigidity for each year are shown in Figs. S19–S21 of the SM [34], respectively. As indicated by the shaded areas of Fig. S19, the 27-day periodicity is most prominent in the second half of 2011, the second half of 2015, the first half of 2016, and the first

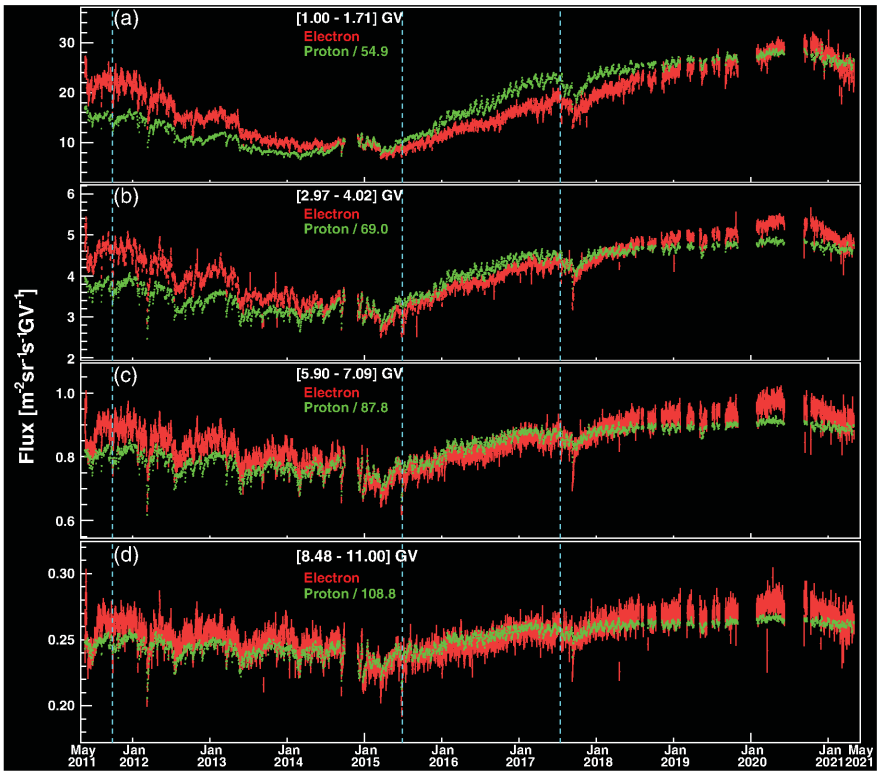

FIG. 1. Eleven-year daily AMS electron fluxes Φ_{e^-} and daily proton fluxes Φ_p in units of [m^{-2} sr^{-1} s^{-1} GV^{-1}] for four rigidity bins from 1.00 to 11.0 GV from May 20, 2011 to November 2, 2021. Days with solar energetic particle events are removed from Φ_p for the lowest rigidity bins shown. The gaps in the fluxes are due to detector studies and upgrades. Note that Φ_p is multiplied by different scale factors as indicated. The scale factor of Φ_p is chosen such that Φ_{e^-} and Φ_p for each rigidity bin are at the same magnitude, on average, during 2014 and 2015. The vertical dashed lines indicate the three time intervals studied in Fig. S7 of the SM [34]. As seen, Φ_{e^-} exhibits large variations with time, and the relative magnitude of these variations [(a)–(d)] decreases with increasing rigidity. The time-dependent behavior of the Φ_{e^-} and Φ_p are distinctly different. From 2011 to 2014, Φ_{e^-} decreases faster with time than Φ_p. From 2015 to mid-2017, Φ_{e^-} increases more slowly than Φ_p below about 4 GV (a),(b). From mid-2020 to 2021, Φ_{e^-} decreases faster than Φ_p.

half of 2017. As seen in Fig. S20, the 13.5-day periodicity is most prominent in the second half of 2011, the second half of 2015, and the second half of 2016. As seen in Fig. S21, the 9-day periodicity is most prominent in the second half of 2015, the first half of 2016, and the second half of 2016.

The rigidity dependence of the strength of all three periodicities varies in different time intervals, but it does not always decrease with increasing rigidity. These observations do not support the paradigm that, over the AMS rigidity range, the strength of the 27-day (and 13.5- and 9-day) periodicities steadily decreases with increasing rigidity of cosmic rays [62].

Figure 2 shows the normalized power as a function of rigidity and period for Φ_{e^-} and Φ_p during two time intervals when the 27-day periodicity is most prominent (second half of 2011 and first half of 2017). As seen, the rigidity dependence behavior of the normalized power of electrons and protons is different in these two time intervals. In particular, in the second half of 2011 [Figs. 2(a) and 2(b)], the strength of the 27-day period of electrons is greater than that of protons, while in the first half of 2017 [Figs. 2(c) and 2(d)], the strength of the 27-day period of electrons is less than that of protons. Figures S22–S24 show the comparison of the peak values of the normalized power including the 95% C.L. between Φ_{e^-} and Φ_p around 27, 13.5, and 9 days, respectively. As seen, the rigidity dependence of the electron periodicities is different from that of protons [30].

The long-term variations on the scale of years are related to the 11- and 22-year cycles of the solar magnetic field [5]. To further investigate the difference in the modulation of Φ_{e^-} and Φ_p, Fig. 3 shows Φ_{e^-} as a function of Φ_p for four rigidity intervals from 1.00 to 11.0 GV. For Figs. 3(a)–3(d), the data points are the daily AMS measurements of Φ_{e^-} and Φ_p. For Figs. 3(e)–3(h), both Φ_{e^-} and Φ_p are calculated with a moving average of 14 BRs with a step of 1 day. Different colors indicate different years from 2011 to 2021. As seen, a hysteresis between Φ_{e^-} and Φ_p is observed; that is, from 2011 to 2018 at a given electron flux, the proton flux shows two distinct branches with time, one before 2014–2015 and one after. Both electron and proton fluxes

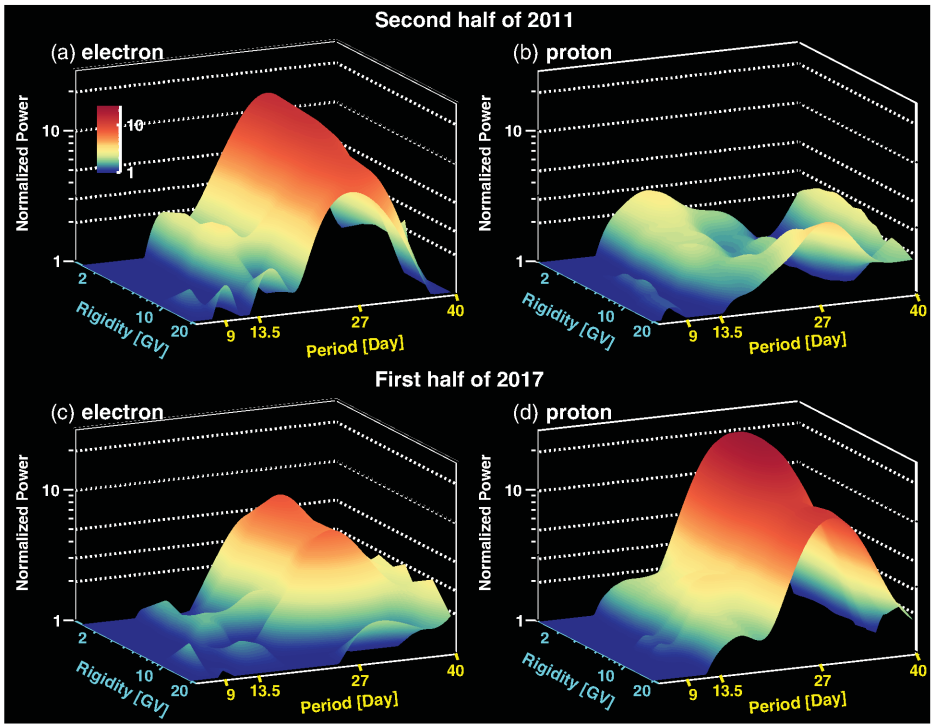

FIG. 2. Normalized power of (a),(c) electron fluxes and (b),(d) proton fluxes as a function of rigidity and time for (a),(b) the second half of 2011 (May 20 to December 16, 2011) and (c),(d) the first half of 2017 (January 22 to July 2, 2017). The rigidity range is from 1.00 to 22.8 GV. As seen, the rigidity dependence behavior of the normalized power of electrons and protons is different in these two time intervals. In particular, in the second half of 2011 [shown in (a) and (b)], the strength of the 27-day period of electrons is greater than that of protons, while in the first half of 2017 [shown in (c) and (d)], the strength of the 27-day period of electrons is less than that of protons.

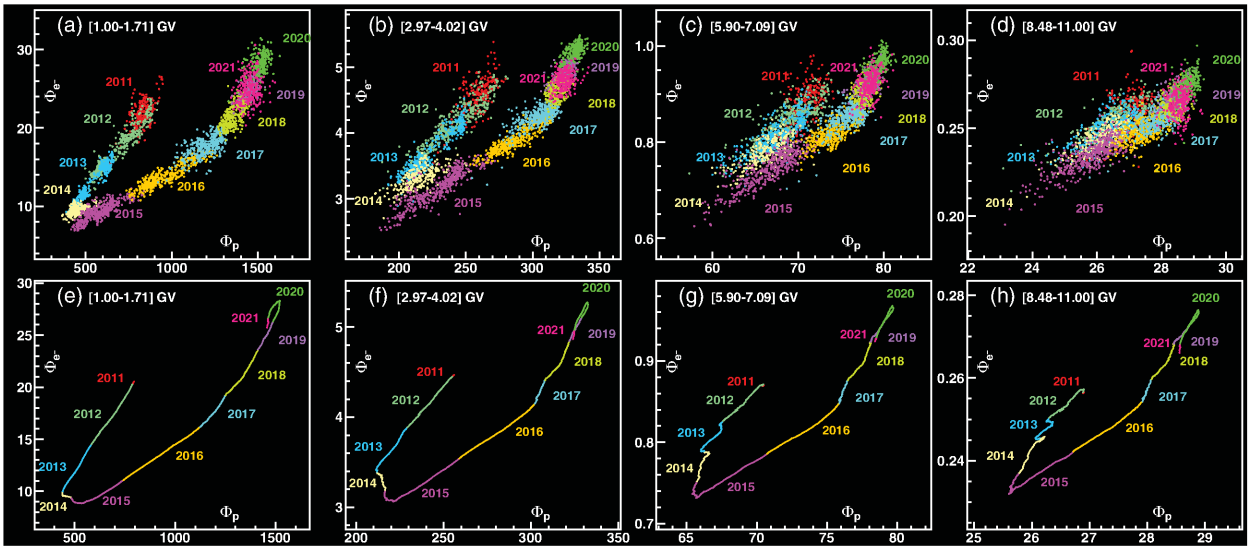

FIG. 3. Electron fluxes Φ_{e^-} versus the proton fluxes Φ_p for four rigidity intervals from 1.00 to 11.0 GV. For (a)–(d), the data points are the daily Φ_{e^-} and Φ_p. For (e)–(h), both Φ_{e^-} and Φ_p are calculated with a moving average of 14 BRs with a step of 1 day. Different colors indicate different years from 2011 to 2021. As seen, a hysteresis between Φ_{e^-} and Φ_p is observed; that is, from 2011 to 2018 at a given electron flux, the proton flux shows two distinct branches with time, one before 2014–2015 and one after. Both Φ_{e^-} and Φ_p peak in 2020, after which the hysteresis curve starts to trace the earlier behavior (2018–2020) backwards. Fluxes are in units of $[\mathrm{m^{-2}\ sr^{-1}\ s^{-1}\ GV^{-1}}]$.

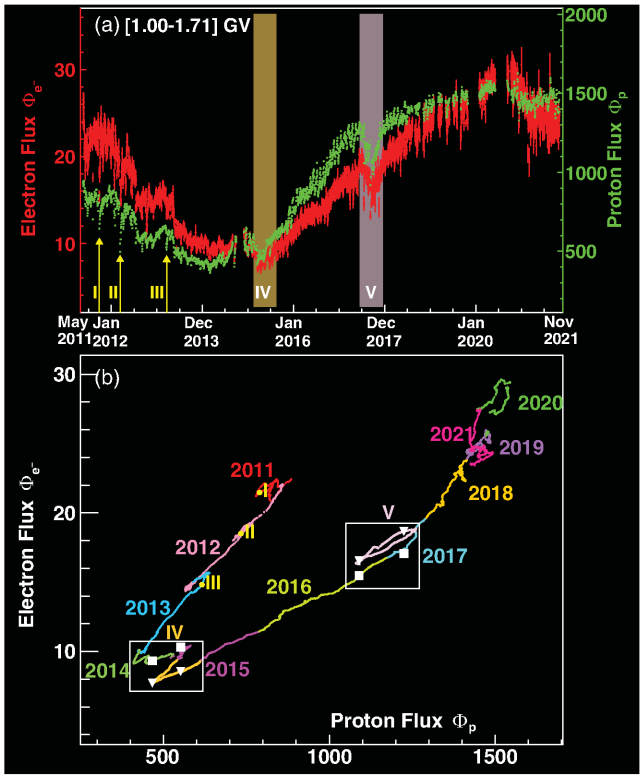

FIG. 4. (a) Daily electron fluxes Φ_{e^-} (red, left axis) and daily proton fluxes Φ_p (green, right axis) as a function of time for the rigidity interval of 1.00 to 1.71 GV. The arrows I, II, and III indicate the location of sharp dips in the proton and electron fluxes, and the colored bands IV and V mark the time intervals around the dips in 2015 and 2017. (b) Φ_{e^-} versus Φ_p both calculated with a moving average of 2 BRs and a step of 1 day. The locations of I, II, and III correspond to the flux dips in (a). To assess the significance of the structures in the hysteresis, during dips IV and V (indicated by white boxes), two pairs (white squares and triangles) of non-overlapping intervals with the same Φ_p but different Φ_{e^-} are chosen. As shown in Fig. S25 of the SM [34], the large dips in 2015 (IV) and 2017 (V) correspond to additional structures in the overall hysteresis with significance of 15.9σ and 7.0σ, respectively. Fluxes are in units of [m^{-2} sr^{-1} s^{-1} GV^{-1}].

peak in 2020, after which the hysteresis curve starts to trace the earlier behavior (2018–2020) backwards. This is consistent with the differences in electron and proton modulation being symmetric with respect to the minimum solar modulation. To assess the significance of this hysteresis, as detailed in the SM [34] (see also Figs. S25 and S26), we study, at different solar conditions, the values of Φ_p at the same Φ_{e^-}. As seen, the hysteresis is observed with a significance of 47σ at [1.00–1.71] GV, greater than 6σ below 8.48 GV, and 4.1σ at [8.48–11.0] GV. Different methods have been used by several independent analysis groups to quantify the significance of the hysteresis, and they show similar results [63].

To probe structures in the hysteresis, the moving averages of the Φ_{e^-} and Φ_p are calculated with a finer time window. The results for the rigidity interval of [1.00–1.71] GV are shown in Fig. 4. Figure 4(a) shows the daily Φ_{e^-} and Φ_p as a function of time for the 11-year period. The arrows I, II, and III indicate the location of sharp dips in the proton and electron fluxes, and the colored bands IV and V mark the time intervals around the dips in 2015 and 2017. The moving average of Φ_{e^-} and Φ_p with the time window of 2 BRs and a step of 1 day for this rigidity interval is shown in Fig. 4(b). The detailed behavior around the dips IV and V is shown in Fig. S27. To assess the significance of these structures in hysteresis, we study the difference of Φ_{e^-} at the same Φ_p; see SM [34] for details. The significance of the hysteresis structure at [1.00–1.71] GV corresponding to the large dip in 2015 is 15.9σ (IV) and to the large dip in 2017 is 7.0σ (V). The analysis at [1.71–2.97] GV is presented in Fig. S28. The significance of the hysteresis structure corresponding to the large dip in 2015 is 14.6σ and to the large dip in 2017 is 5.3σ.

The structures in the hysteresis in 2015 and 2017 are likely caused by a series of interplanetary coronal mass ejections [64]. The clear deviation from the long-term trend implies a charge-sign-dependent modulation during those solar transients on the timescale of several Bartels rotations.

In conclusion, we presented the precision measurements of 11 years of daily cosmic electron fluxes in the rigidity interval from 1.00 to 41.9 GV based on 2.0×10^8 electrons. The electron fluxes exhibit variations on multiple timescales. In the 11-year period, the electron fluxes show distinctly different time variations from the proton fluxes. Recurrent electron flux variations with periods of 27 days, 13.5 days, and 9 days are observed. The strength of all three periods of electron fluxes shows different rigidity and time dependence compared to protons. Remarkably, a hysteresis between the electron flux and the proton flux is observed with a significance greater than 6σ at rigidities below 8.5 GV. Furthermore, significant structures in the electron-proton hysteresis are observed, corresponding to sharp variations in the fluxes. These continuous daily electron data provide unique input to the understanding of the charge sign dependence of cosmic rays over an 11-year solar cycle.

We are grateful for important physics discussions with Igor Moskalenko. We thank former NASA Administrator Daniel S. Goldin for his dedication to the legacy of the ISS as a scientific laboratory and his decision for NASA to fly AMS as a DOE payload. We also acknowledge the continuous support of the NASA leadership, particularly Kathryn Lueders, and of the JSC and MSFC flight control teams that have allowed AMS to operate optimally on the ISS for over 11 years. We are grateful for the support of Glen Crawford of the DOE including resources from the National Energy Research Scientific Computing Center under Contract No. DE-AC02-05CH11231. We gratefully acknowledge strong support from CERN, including Fabiola Gianotti, and the CERN IT department, including

Bernd Panzer-Steindel. We also acknowledge the continuous support from MIT and its School of Science, Nergis Mavalvala, and the Laboratory for Nuclear Science, Boleslaw Wyslouch. Research supported by the following: Chinese Academy of Sciences, Institute of High Energy Physics, Institute of Electrical Engineering, China Academy of Space Technology, National Natural Science Foundation, and Ministry of Science and Technology, the China Scholarship Council, the provincial governments of Shandong, Jiangsu, Guangdong, Shandong University, and the Shandong Institute of Advanced Technology, China; the Academy of Finland, Project No. 321882, Finland; CNRS/IN2P3 and CNES, France; DLR under Grant No. 50OO1805 and computing support on the JARA Partition of the RWTH Aachen supercomputer, Germany; INFN and ASI under ASI-INFN Agreements No. 2019-19-HH.0, its amendments, and No. 2021-43-HH.0, and ASI-University of Perugia Agreement No. 2019-2-HH.0, Italy; CHEP and NRF under Grant No. NRF-2018R1A6A1A06024970 at Kyungpook National University, Korea; the Consejo Nacional de Ciencia y Tecnología and UNAM, Mexico; NWO under Grant No. 680-1-004, Netherlands; FCT under Grant No. CERN/FIS-PAR/0013/2019, Portugal; the Ministry of Science and Higher Education under Project No. 0723-2020-0040, Russia; CIEMAT, IAC, CDTI, and SEIDI-MINECO under Grants No. PID2019–107988 GB-C21/C22 and No. CEX2019-000920-S, Spain; the Fondation Dr. Manfred Steuer, Switzerland; Academia Sinica and the Ministry of Science and Technology (MOST) under Grants No. 107-2119-M-006-015-MY3, No. 109-2112-M-001-029, and No. CDA-105-M06, former Presidents of Academia Sinica, Yuan-Tseh Lee and Chi-Huey Wong, and former Ministers of MOST, Maw-Kuen Wu and Luo-Chuan Lee, Taiwan; the Turkish Energy, Nuclear and Mineral Research Agency (TENMAK) under Grant No. 2020TAEK(CERN)A5.H1.F5-26, Turkey; and NSF Grants No. 1455202 and No. 2013228, Wyle Laboratories Grant No. 2014/T72497, and NASA NESSF Grant No. HELIO15F-0005, USA.

[*]Also at Nikhef, 1098 XG Amsterdam, Netherlands.
[†]Also at IRCCS Azienda Ospedaliero-Universitaria di Bologna, Bologna, Italy.

[1] A. W. Strong and I. V. Moskalenko, Propagation of cosmic-ray nucleons in the galaxy, Astrophys. J. **509**, 212 (1998); A. E. Vladimirov, S. W. Digel, G. Jóhannesson, P. F. Michelson, I. V. Moskalenko, P. L. Nolan, E. Orlando, T. A. Porter, and A. W. Strong, GALPROP WebRun: An internet-based service for calculating galactic cosmic ray propagation and associated photon emissions, Comput. Phys. Commun. **182**, 1156 (2011).

[2] C. Evoli, D. Gaggero, A. Vittino, G. Di Bernardo, M. Di Mauro, A. Ligorini, P. Ullio, and D. Grasso, Cosmic-ray propagation with DRAGON2: I. Numerical solver and astrophysical ingredients, J. Cosmol. Astropart. Phys. 02 (2017) 015.

[3] D. Maurin, F. Donato, R. Taillet, and P. Salati, Cosmic rays below $Z = 30$ in a diffusion model: New constraints on propagation parameters, Astrophys. J. **555**, 585 (2001).

[4] A. Putze, L. Derome, and D. Maurin, A Markov chain Monte Carlo technique to sample transport and source parameters of galactic cosmic rays II. Results for the diffusion model combining B/C and radioactive nuclei, Astron. Astrophys. **516**, A66 (2010).

[5] M. S. Potgieter, Solar modulation of cosmic rays, Living Rev. Solar Phys. **10**, 3 (2013).

[6] E. N. Parker, The passage of energetic charged particles through interplanetary space, Planet. Space Sci. **13**, 9 (1965).

[7] M. S. Potgieter, The charge-sign dependent effect in the solar modulation of cosmic rays, Adv. Space Res. **53**, 1415 (2014).

[8] M. Aguilar *et al.*, The Alpha Magnetic Spectrometer (AMS) on the international space station: Part II—Results from the first seven years, Phys. Rep. **894**, 1 (2021).

[9] P. D. Serpico, Astrophysical models for the origin of the positron "excess", Astropart. Phys. **39**, 2 (2012); T. Linden and S. Profumo, Probing the pulsar origin of the anomalous positron fraction with AMS-02 and atmospheric Cherenkov telescopes, Astrophys. J. **772**, 18 (2013); I. Cholis and D. Hooper, Dark matter and pulsar origins of the rising cosmic ray positron fraction in light of new data from the AMS, Phys. Rev. D **88**, 023013 (2013); D. Hooper, I. Cholis, T. Linden, and K. Fang, HAWC observations strongly favor pulsar interpretations of the cosmic-ray positron excess, Phys. Rev. D **96**, 103013 (2017); S. Profumo, J. Reynoso-Cordova, N. Kaaz, and M. Silverman, Lessons from HAWC pulsar wind nebulae observations: The diffusion constant is not a constant; pulsars remain the likeliest sources of the anomalous positron fraction; cosmic rays are trapped for long periods of time in pockets of inefficient diffusion, Phys. Rev. D **97**, 123008 (2018).

[10] P. Mertsch and S. Sarkar, AMS-02 data confront acceleration of cosmic ray secondaries in nearby sources, Phys. Rev. D **90**, 061301(R) (2014); N. Tomassetti and F. Donato, The connection between the positron fraction anomaly and the spectral features in the galactic cosmic-ray hadrons, Astrophys. J. Lett. **803**, L15 (2015); W. Liu, X. J. Bi, S. J. Lin, B. B. Wang, and P. F. Yin, Excesses of cosmic ray spectra from a single nearby source, Phys. Rev. D **96**, 023006 (2017); M. Kachelrieß, A. Neronov, and D. V. Semikoz, Cosmic ray signatures of a 2–3 Myr old local supernova, Phys. Rev. D **97**, 063011 (2018).

[11] M. S. Turner and F. Wilczek, Positron line radiation as a signature of particle dark matter in the halo, Phys. Rev. D **42**, 1001 (1990); J. Ellis, Particles and cosmology: Learning from cosmic rays, AIP Conf. Proc. **516**, 21 (2000); H. C. Cheng, J. L. Feng, and K. T. Matchev, Kaluza-Klein Dark Matter, Phys. Rev. Lett. **89**, 211301 (2002); G. Kane, R. Lu, and S. Watson, PAMELA satellite data as a signal of non-thermal wino LSP dark matter, Phys. Lett. B **681**, 151 (2009); J. Kopp, Constraints on dark matter annihilation from AMS-02 results, Phys. Rev. D **88**, 076013 (2013); C. H. Chen, C. W. Chiang, and T. Nomura, Dark matter for excess of AMS-02 positrons and antiprotons, Phys. Lett. B

747, 495 (2015); H. C. Cheng, W. C. Huang, X. Huang, I. Low, Y. L. Sming Tsai, and Q. Yuan, AMS-02 positron excess and indirect detection of three-body decaying dark matter, J. Cosmol. Astropart. Phys. 03 (2017) 041; Y. Bai, J. Berger, and S. Lu, Supersymmetric resonant dark matter: A thermal model for the AMS-02 positron excess, Phys. Rev. D 97, 115012 (2018).

[12] M. Cirelli, D. Gaggero, G. Giesen, M. Taoso, and A. Urbano, Antiproton constraints on the GeV gamma-ray excess: A comprehensive analysis, J. Cosmol. Astropart. Phys. 12 (2014) 045.

[13] N. Tomassetti, M. Orcinha, F. Barao, and B. Bertucci, Evidence for a time lag in solar modulation of galactic cosmic rays, Astrophys. J. Lett. 849, L32 (2017).

[14] V. Di Felice, R. Munini, E. E. Vos, and M. S. Potgieter, New evidence for charge-sign-dependent modulation during the solar minimum of 2006 to 2009, Astrophys. J. 834, 89 (2017).

[15] M. S. Potgieter and E. E. Vos, Difference in the heliospheric modulation of cosmic-ray protons and electrons during the solar minimum period of 2006 to 2009, Astron. Astrophys. 601, A23 (2017).

[16] R. Manuel, S. E. S. Ferreira, and M. S. Potgieter, Time-dependent modulation of cosmic rays in the heliosphere, Sol. Phys. 289, 2207 (2014).

[17] M. Aguilar *et al.*, Towards Understanding the Origin of Cosmic-Ray Positrons, Phys. Rev. Lett. 122, 041102 (2019).

[18] M. Aguilar *et al.*, Towards Understanding the Origin of Cosmic-Ray Electrons, Phys. Rev. Lett. 122, 101101 (2019).

[19] A. W. Strong, I. V. Moskalenko, and V. S. Ptuskin, Cosmic-ray propagation and interactions in the galaxy, Annu. Rev. Nucl. Part. Sci. 57, 285 (2007).

[20] M. Jubelgas, V. Springel, T. Enßlin, and C. Pfrommer, Cosmic ray feedback in hydrodynamical simulations of galaxy formation, Astron. Astrophys. 481, 33 (2008).

[21] M. Zhang, P. Zuo, and N. Pogorelov, Heliospheric influence on the anisotropy of TeV cosmic rays, Astrophys. J. 790, 5 (2014).

[22] M. J. Boschini *et al.*, Solution of heliospheric propagation: Unveiling the local interstellar spectra of cosmic-ray species, Astrophys. J. 840, 115 (2017); M. J. Boschini *et al.*, HelMod in the works: From direct observations to the local interstellar spectrum of cosmic-ray electrons, Astrophys. J. 854, 94 (2018).

[23] M. Garcia-Munoz, P. Meyer, K. R. Pyle, and J. A. Simpson, The dependence of solar modulation on the sign of the cosmic ray particle charge: Further study of a 22 year solar magnetic cycle, in *Proceedings of the 20th International Cosmic Ray Conference* (Nauka, Moscow, Soviet Union, 1987), Vol. 3, p. 303; M. Garcia-Munoz, P. Meyer, K. R. Pyle, J. A. Simpson, P. Evenson, J. Esposito, and E. Tuska, The dependence of solar modulation on the sign of the cosmic ray particle charge during the 22-year solar magnetic cycle, in *Proceedings of the 22nd International Cosmic Ray Conference* (Dublin Institute for Advanced Studies, Dublin, Ireland, 1991), Vol. 3, p. 497; P. Evenson, Cosmic ray electrons, *Cosmic Rays in the Heliosphere* (Springer, New York, 1998), pp. 63–73.

[24] J. M. Clem, D. P. Clements, J. Esposito, P. Evenson, D. Huber, J. L'Heureux, P. Meyer, and C. Constantin, Solar modulation of cosmic electrons, Astrophys. J. 464, 507 (1996).

[25] B. Heber *et al.*, Ulysses cosmic ray and solar particle investigation/Kiel electron telescope observations: Charge sign dependence and spatial gradients during the 1990–2000 $A > 0$ solar magnetic cycle, J. Geophys. Res. 107, 1274 (2002); B. Heber *et al.*, Modulation of galactic cosmic ray protons and electrons during an unusual solar minimum, Astrophys. J. 699, 1956 (2009); B. Heber, Cosmic rays through the solar Hale cycle, Space Sci. Rev. 176, 265 (2013).

[26] F. Alemanno *et al.*, Observations of Forbush decreases of cosmic-ray electrons and positrons with the dark matter particle explorer, Astrophys. J. Lett. 920, L43 (2021).

[27] O. Adriani *et al.*, Time dependence of the e^- flux measured by PAMELA during the 2006 July—2009 December solar minimum, Astrophys. J. 810, 142 (2015); O. Adriani *et al.*, Time Dependence of the Electron and Positron Components of the Cosmic Radiation Measured by the PAMELA Experiment between July 2006 and December 2015, Phys. Rev. Lett. 116, 241105 (2016).

[28] R. Munini *et al.*, Evidence of energy and charge sign dependence of the recovery time for the 2006 December Forbush event measured by the PAMELA experiment, Astrophys. J. 853, 76 (2018).

[29] M. Aguilar *et al.*, Observation of Complex Time Structures in the Cosmic-Ray Electron and Positron Fluxes with the Alpha Magnetic Spectrometer on the International Space Station, Phys. Rev. Lett. 121, 051102 (2018).

[30] M. Aguilar *et al.*, Periodicities in the Daily Proton Fluxes from 2011 to 2019 Measured by the Alpha Magnetic Spectrometer on the International Space Station from 1 to 100 GV, Phys. Rev. Lett. 127, 271102 (2021).

[31] M. Aguilar *et al.*, Properties of Daily Helium Fluxes, Phys. Rev. Lett. 128, 231102 (2022).

[32] X. Sun, J. T. Hoeksema, Y. Liu, and J. Zhao, On polar magnetic field reversal and surface flux transport during solar cycle 24, Astrophys. J. 798, 114 (2015).

[33] A. Kounine, The Alpha Magnetic Spectrometer on the International Space Station, Int. J. Mod. Phys. E 21, 1230005 (2012); S. Rosier-Lees, New results from AMS, in *Proceedings of the Astroparticle Physics TEVPA/IDM, Amsterdam, 2014* (unpublished); S. Ting, The alpha magnetic spectrometer on the international space station, Nucl. Phys. B, Proc. Suppl. 243–244, 12 (2013); S.-C. Lee, Latest results from AMS, in *Proceedings of the 20th International Conference on Supersymmetry and Unification of Fundamental Interactions (SUSY 2012), Beijing, 2012* (unpublished); M. Aguilar, The AMS experiment on the ISS, in *Proceedings of the XL International Meeting on Fundamental Physics, Centro de Ciencias de Benasque Pedro Pascual, 2012* (unpublished); S. Schael, Status of the AMS-02 experiment on the ISS, in *Proceedings of the 10th Symposium on Sources and Detection of Dark Matter and Dark Energy in the Universe, Los Angeles, 2012* (unpublished); B. Bertucci, The AMS-02 detector operation in space, Proc. Sci. EPS-HEP2011 (2011) 67; M. Incagli, Astroparticle physics with AMS02, AIP Conf. Proc. 1223,

43 (2010); R. Battiston, The Antimatter Spectrometer (AMS-02): A particle physics detector in space, Nucl. Instrum. Methods Phys. Res., Sect. A **588**, 227 (2008).

[34] See Supplemental Material at http://link.aps.org/supplemental/10.1103/PhysRevLett.130.161001 for the AMS detector description, details of event selection, definition of years, explanation of the dip in 2015 and 2017, details of wavelet analysis, hysteresis analysis, figures, and the tabulated daily electron fluxes as functions of rigidity.

[35] K. Lübelsmeyer *et al.*, Upgrade of the Alpha Magnetic Spectrometer (AMS-02) for long term operation on the International Space Station (ISS), Nucl. Instrum. Methods Phys. Res., Sect. A **654**, 639 (2011).

[36] B. Alpat *et al.*, The internal alignment and position resolution of the AMS-02 silicon tracker determined with cosmic-ray muons, Nucl. Instrum. Methods Phys. Res., Sect. A **613**, 207 (2010).

[37] G. Ambrosi, V. Choutko, C. Delgado, A. Oliva, Q. Yan, and Y. Li, The spatial resolution of the silicon tracker of the Alpha Magnetic Spectrometer, Nucl. Instrum. Methods Phys. Res., Sect. A **869**, 29 (2017).

[38] Y. Jia, Q. Yan, V. Choutko, H. Liu, and A. Oliva, Nuclei charge measurement by the Alpha Magnetic Spectrometer silicon tracker, Nucl. Instrum. Methods Phys. Res., Sect. A **972**, 164169 (2020).

[39] F. Hauler *et al.*, The AMS-02 TRD for the international space station, IEEE Trans. Nucl. Sci. **51**, 1365 (2004); Ph. Doetinchem *et al.*, Performance of the AMS-02 transition radiation detector, Nucl. Instrum. Methods Phys. Res., Sect. A **558**, 526 (2006); Th. Kirn, The AMS-02 TRD on the international space station, Nucl. Instrum. Methods Phys. Res., Sect. A **706**, 43 (2013).

[40] V. Bindi *et al.*, Calibration and performance of the AMS-02 time of flight detector in space, Nucl. Instrum. Methods Phys. Res., Sect. A **743**, 22 (2014).

[41] C. Adloff *et al.*, The AMS-02 lead-scintillating fibres electromagnetic calorimeter, Nucl. Instrum. Methods Phys. Res., Sect. A **714**, 147 (2013); A. Kounine, Z. Weng, W. Xu, and C. Zhang, Precision measurement of 0.5 GeV–3 TeV electrons and positrons using the AMS electromagnetic calorimeter, Nucl. Instrum. Methods Phys. Res., Sect. A **869**, 110 (2017).

[42] J. Allison *et al.*, Recent developments in GEANT4, Nucl. Instrum. Methods Phys. Res., Sect. A **835**, 186 (2016); J. Allison *et al.*, GEANT4 developments and applications, IEEE Trans. Nucl. Sci. **53**, 270 (2006); S. Agostinelli *et al.*, GEANT4–A simulation toolkit, Nucl. Instrum. Methods Phys. Res., Sect. A **506**, 250 (2003).

[43] Q. Yan, V. Choutko, A. Oliva, and M. Paniccia, Measurements of nuclear interaction cross sections with the Alpha Magnetic Spectrometer on the International Space Station, Nucl. Phys. **A996**, 121712 (2020).

[44] M. Aguilar *et al.* (AMS Collaboration), Measurement of the geomagnetic cutoff with the Alpha Magnetic Spectrometer on the International Space Station (to be published).

[45] C. C. Finlay *et al.*, International geomagnetic reference field: The eleventh generation, Geophys. J. Int. **183**, 1216 (2010); E. Thébault *et al.*, International geomagnetic reference field: The 12th generation, Earth Planets Space **67**, 79 (2015); Geomagnetic field modeling working group, IGRF-13 model (2019), https://www.ngdc.noaa.gov/IAGA/vmod/igrf.html.

[46] P. Bobik, G. Boella, M. J. Boschini, D. Grandi, M. Gervasi, K. Kudela, S. Pensotti, and P. G. Rancoita, Magnetospheric transmission function approach to disentangle primary from secondary cosmic ray fluxes in the penumbra region, J. Geophys. Res. **111**, A05205 (2006); N. A. Tsyganenko and M. I. Sitnov, Modeling the dynamics of the inner magnetosphere during strong geomagnetic storms, J. Geophys. Res. **110**, A03208 (2005).

[47] M. Aguilar *et al.*, Precision Measurement of the Proton Flux in Primary Cosmic Rays from Rigidity 1 GV to 1.8 TV with the Alpha Magnetic Spectrometer on the International Space Station, Phys. Rev. Lett. **114**, 171103 (2015).

[48] J. Berdugo, V. Choutko, C. Delgado, and Q. Yan, Determination of the rigidity scale of the Alpha Magnetic Spectrometer, Nucl. Instrum. Methods Phys. Res., Sect. A **869**, 10 (2017).

[49] Note that the data can also be downloaded in different formats from the AMS website https://ams02.space/sites/default/files/publication/202209/table-s1-s3300.csv, the ASI cosmic-ray database at https://tools.ssdc.asi.it/CosmicRays, and the LPSC cosmic-ray database at https://lpsc.in2p3.fr/crdb/.

[50] S. E. Forbush, On cosmic-ray effects associated with magnetic storms, Terr. Magn. Atmos. Electr. **43**, 203 (1938).

[51] M. Zhang, Modulation of galactic cosmic rays at solar maximum: Observations, Adv. Space Res. **32**, 603 (2003); H. V. Cane, Coronal mass ejections and Forbush decreases, Space Sci. Rev. **93**, 55 (2000); M. S. Potgieter, J. A. Le Roux, L. F. Burlaga, and F. B. McDonald, The role of merged interaction regions and drifts in the heliospheric modulation of cosmic rays beyond 20 AU: A computer simulation, Astrophys. J. **403**, 760 (1993); G. Wibberenz, I. G. Richardson, and H. V. Cane, A simple concept for modeling cosmic ray modulation in the inner heliosphere during solar cycles 20–23, J. Geophys. Res. **107**, 1353 (2002).

[52] J. A. Simpson, A brief history of recurrent solar modulation of the galactic cosmic rays (1937–1990), Space Sci. Rev. **83**, 169 (1998).

[53] C. Paizis *et al.*, Amplitude evolution and rigidity dependence of the 26-day recurrent cosmic ray decreases: COSPIN/KET results, J. Geophys. Res. **104**, 28241 (1999).

[54] Z. Shen, G. Qin, P. Zuo, F. Wei, and X. Xu, A study of variations of galactic cosmic-ray intensity based on a hybrid data-processing method, Astrophys. J. **900**, 143 (2020).

[55] R. Modzelewska *et al.*, Study of the 27 day variations in GCR fluxes during 2007-2008 based on PAMELA and ARINA observations, Astrophys. J. **904**, 3 (2020). In this Letter, the rigidity dependence of the 27-day periodicity in 2007-2008 has been directly measured.

[56] R. Modzelewska and A. Gil, Recurrence of galactic cosmic-ray intensity and anisotropy in solar minima 23/24 and 24/25 observed by ACE/CRIS, STEREO, SOHO/EPHIN and neutron monitors, Astron. Astrophys. **646**, A128 (2021).

[57] A. López-Comazzi and J. J. Blanco, Short-term periodicities observed in neutron monitor counting rates, Sol. Phys. **295**, 81 (2020).

[58] M. Armano *et al.*, Characteristics and energy dependence of recurrent galactic cosmic-ray flux depressions and of a Forbush decrease with LISA pathfinder, Astrophys. J. **854**, 113 (2018).

[59] I. Sabbah and K. Kudela, Third harmonic of the 27 day periodicity of galactic cosmic rays: Coupling with interplanetary parameters, J. Geophys. Res. **116**, A04103 (2011).

[60] M. Temmer, B. Vršnak, and A. M. Veronig, Periodic appearance of coronal holes and the related variation of solar wind parameters, Sol. Phys. **241**, 371 (2007).

[61] C. Torrence and G. P. Compo, A practical guide to wavelet analysis, Bull. Am. Meteorol. Soc. **79**, 61 (1998).

[62] A. Gil and M. V. Alania, Theoretical and experimental studies of the rigidity spectrum of the 27-day variation of the galactic cosmic ray intensity in different epochs of solar activity, Sol. Phys. **283**, 565 (2013); A. López-Comazzi and J. J. Blanco, Short-term periodicities observed in neutron monitor counting rates, Sol. Phys. **295**, 81 (2020).

[63] M. Aguilar *et al.* (AMS Collaboration), Eleven years of AMS physics results on the International Space Station [Rev. Mod. Phys. (to be published)].

[64] I. Richardson and H. Cane, Near-Earth interplanetary coronal mass ejections since January 1996, https://izw1.caltech.edu/ACE/ASC/DATA/level3/icmetable2.htm, specifically the events starting from March 16, 2015 and from July 16, 2017.